Original

VIRGO	PJT930211	
R. Flaminio H. Heitmann 22/11/93	Subject : **Interferometer locking scheme**	

I Introduction

The aim of this note is to report the status of the work done during the last six months on the locking scheme for the VIRGO interferometer.

It is well known that a free suspended mirror oscillates around its equilibrium point at very low frequency with a (variable) amplitude of some tens of a wavelength. A local damping system may reduce this amplitude to a fraction of a wavelength which, however, is not sufficient for the precision required. Moreover, it does not help against slow, e.g. thermal, drifts. Thus, purely local systems are not sufficient to maintain the interferometer at the working position, so that a global control system is necessary to lock the interferometer.

A sketch of the interferometer with the six main optical components (recycling mirror M_r, beam splitter M_s and the four cavity mirrors M_{11}, M_{12}, M_{21} and M_{22}) defining its geometry is shown in fig. 1.1. Locking the interferometer means keeping the two Fabry-Perot cavities as well as the recycling cavity in resonance with the laser source and the interferometer output on the dark fringe. This means that there are four independent lengths that need being controlled: the two Fabry-Perot cavity lengths (L_1 and L_2), the recycling cavity length ($l_0 + (l_1+l_2) / 2$) and the Michelson arm length difference (l_1-l_2). The problem is to extract four independent error signals related to these four lengths and to feed them back to the various mirrors. This feedback

system must have a high gain at very low frequency (let's say up to 1Hz), and should not introduce noise in the operating frequency range of the antenna (10Hz-1kHz).

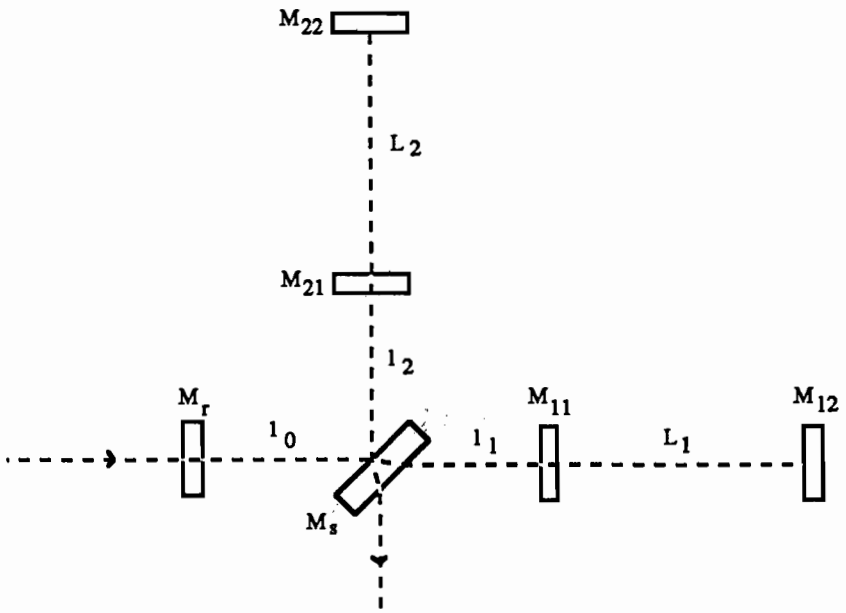

Fig. 1.1

In order to keep the recycling cavity at the resonance condition, the recycling mirror position (or better its position relative to the cavity input mirrors) should be controlled with an accuracy of $8 \cdot 10^{-4}\ \lambda$ (HWHM of the recycling cavity). In order to maintain the whole interferometer in resonance with the laser frequency the cavity mirror positions (or better their relative positions) should be controlled with an accuracy of $3 \cdot 10^{-5}\ \lambda$. If one wants to keep the interferometer output on the dark fringe with a precision of 10^{-3} rad this accuracy must be increased by a factor of ten ($3 \cdot 10^{-6}\ \lambda$). This same request imposes an accuracy of $8 \cdot 10^{-5}\ \lambda$ on the beam splitter position.

As already said, the feedback system should not introduce additional noise at the working frequencies of the antenna. The specifications, calculated for a noise level three times below the VIRGO goals ($h=10^{-21}$ @ 10Hz and $h=3 \cdot 10^{-23}$ @ 100Hz), are given in the following table (see also ref [1]); for the recycling mirror the specifications have been calculated assuming that the laser frequency is stabilised on the recycling cavity.

	10 Hz	100 Hz
Cavity mirr.	6.10^{-19} m/$\sqrt{\text{Hz}}$	2.10^{-20} m/$\sqrt{\text{Hz}}$
Beam Splitter	$1.5\ 10^{-17}$ m/$\sqrt{\text{Hz}}$	5.10^{-19} m/$\sqrt{\text{Hz}}$
Recycling mirr.	2.10^{-15} m/$\sqrt{\text{Hz}}$	7.10^{-17} m/$\sqrt{\text{Hz}}$

As already said, the problem consists in extracting four error signals related to the four lengths that must be controlled. In order to avoid the noise due to laser power fluctuations at

low frequencies[2,3], the measurement must be shifted to the quieter MHz domain using a modulation-demodulation technique. The laser light is phase modulated and the signals will be extracted by demodulating the photodiode currents at the various outputs of the interferometer.

Various modulation configurations for the extraction of the gravitational wave signal were proposed and studied in the past (for a short review see ref. [2]). One of them, known as internal modulation [3,4], consists in modulating the laser beam inside the two Michelson arms (fig. 1.2) and demodulating at the output of the interferometer. The use of modulators inside the interferometer arms has several drawbacks. They usually introduce wave front distortions that decrease the interferometer contrast. Furthermore they may have losses that can limit the recycling factor. Finally it can be difficult to fabricate modulators capable of supporting the very high power beam typical of VIRGO. All these problems prevent the use of this solution.

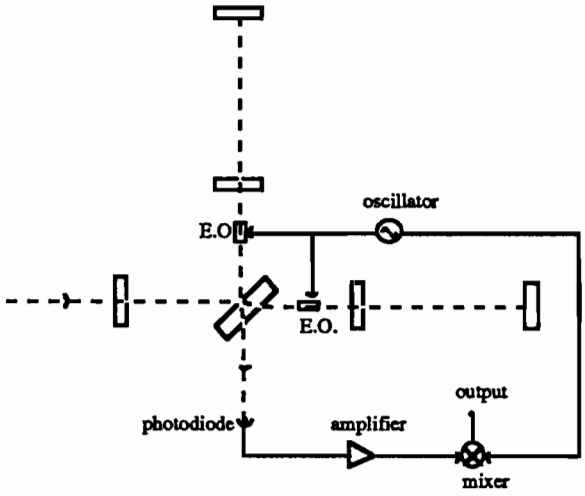

Fig. 1.2

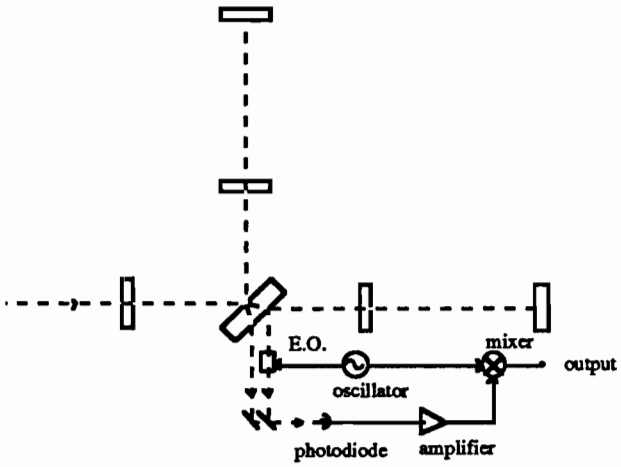

Fig. 1.3

The second one, called external modulation [5,6], is the one proposed for VIRGO in the FCD [7]. It consists in extracting one auxiliary beam from the anti-reflection coated face of the beam splitter, phase modulating it and mixing it with the main interference as in a Mach-Zehnder interferometer (fig. 1.3). This solution needs additional optical components that, in order to avoid noise, must be suspended [8]. Furthermore, it introduces one more variable (the length of the second Mach-Zehnder arm), which must be controlled. This complicates the realisation of this scheme and is the reason that induced us to study a third method, first proposed by Schnupp [9], known as frontal modulation.

II Frontal Modulation

In the frontal modulation configuration [10] the laser beam is phase-modulated at the input of the interferometer (fig. 2.1). The short Michelson arms (l_1,l_2) are somewhat asymmetric, such that the dark fringe condition is, as before, fulfilled for the carrier, but no longer for the modulation side bands, which now partially impinge on the detector. If, e.g. by a gravitational wave, the dark fringe condition gets disturbed, a small part of the carrier leaks out with a phase shift of 90°, so that its beat with the side bands creates an amplitude modulated diode current, which can be detected by mixing with the modulation frequency, as before.

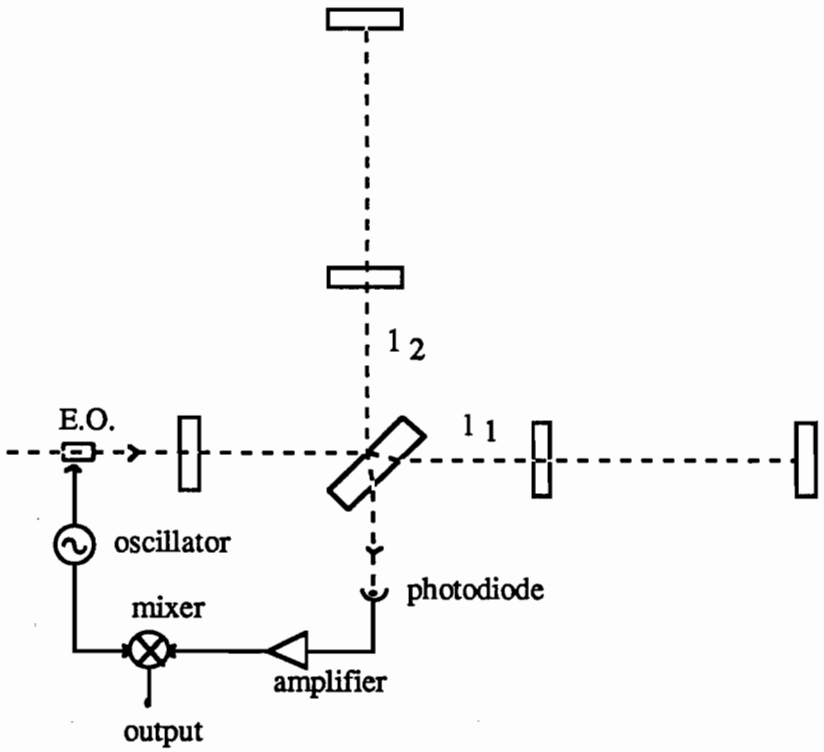

Fig. 2.1

The frequency of modulation Ω has to be chosen so that the two first order sidebands are not reflected by the recycling cavity. Otherwise the effective modulation depth inside the interferometer will be strongly depressed. Mathematically this is expressed by the following condition:

$$-\frac{\Omega\, l_r}{c} + \Phi_c(\omega \pm \Omega) = \pi \pmod{2\pi} \qquad (2.1)$$

where Φ_c is the phase reflectivity of the long Fabry-Perot's and l_r is the mean recycling cavity length:

$$l_r = l_0 + \frac{l_1+l_2}{2} \qquad (2.2)$$

Figures (2.2) and (2.3) show the sideband amplitudes inside the recycling cavity as a function of the modulation frequency Ω. The two figures correspond to two different domains of frequencies. In both graphs we see various peaks corresponding to those frequencies that satisfy condition (2.1). The distance between the peaks varies in accordance with the frequency domain we are considering but it is always nearly equal to the free spectral range of the long Fabry Perot ($\approx$ 50 kHz).

In the first graph the peaks correspond to a modulation frequency which is also resonant inside the long Fabry-Perot's. Consequently a little variation of the frequency value introduces an additional phase factor that takes the sidebands out of resonance. This explains why the peaks are so thin (a few Hertz). In the second graph the peaks correspond to a frequency of modulation which is anti-resonant in the Fabry-Perot's and consequently they are larger.

For a given modulation frequency there is an optimum length difference Δl between the two arms of the Michelson which maximises the transmission of the sidebands to the output port of the interferometer. This is given by the following condition (see appendix A):

$$\cos\left(\frac{\Omega\ \Delta l}{c}\right) = r_r\, r_{ITF}\ , \qquad (2.3)$$

r_r being the recycling mirror amplitude reflectivity and r_{ITF} the reflectivity of the whole interferometer without the recycling mirror. The physical interpretation of (2.3) is that the side band power extracted equals the power lost inside the recycling cavity (optimum output coupling condition).

Figures (2.4) and (2.5) show the sideband transmission amplitude as a function of Δl, respectively, for $\Omega \approx$ 12.5 MHz (resonant in the Fabry-Perot's) and $\Omega \approx$ 6.27 MHz (not resonant in the Fabry-Perot's). In both cases we see that condition (2.3) is not very strict, and that optimum values for Δl are in the range of 0.5-0.8 m which are not very big asymmetries.

For a given Δl the sideband amplitudes at the output port of the interferometer may be varied by varying the phase modulation amplitude. The graph (2.6) represents the signal-to-noise ratio as a function of the modulation amplitude m for a contrast defect equal to 10^{-4}. As it is shown in the figure it exists an optimum modulation amplitude that, for a given contrast, maximises the signal-to-noise ratio. Nevertheless the maximum is quite broad so that one does not have to fit exactly this condition.

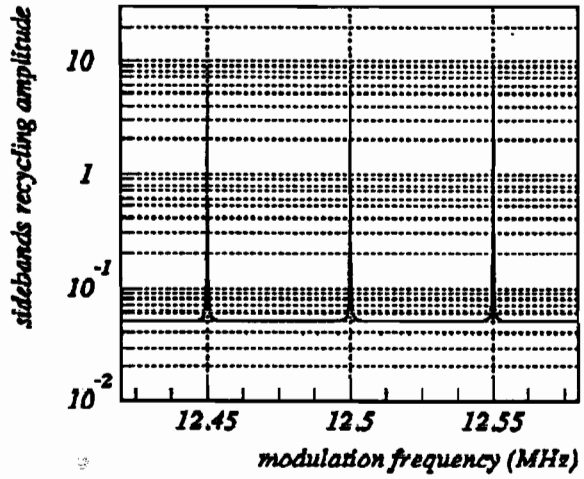

fig. 2.2

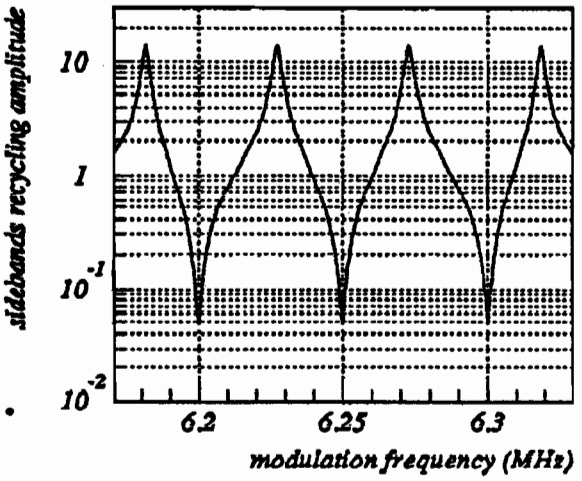

fig. 2.3

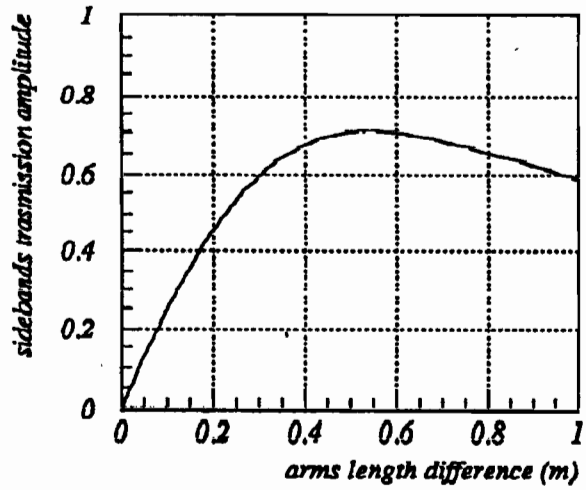

fig. 2.4

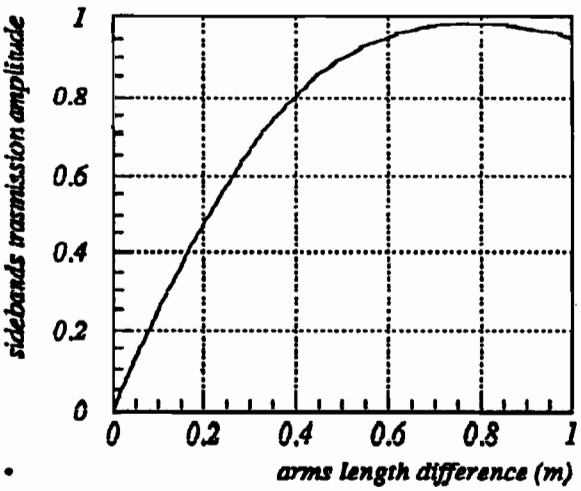

fig. 2.5

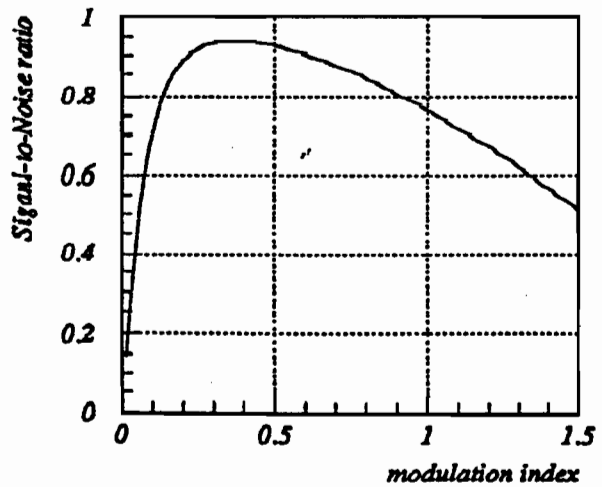

fig. 2.6

III Locking Scheme with Simple Frontal Modulation

As already said, in order to lock the interferometer one needs four independent signals related to the four degrees of freedom that need being controlled. In the following we will describe the interferometer displacements on the following base: Fabry-Perot's common mode (fig.3.1.a), Fabry-Perot's differential mode (fig.3.1.b), Michelson common mode (fig.3.1.c) and Michelson differential mode (fig.3.1.d).

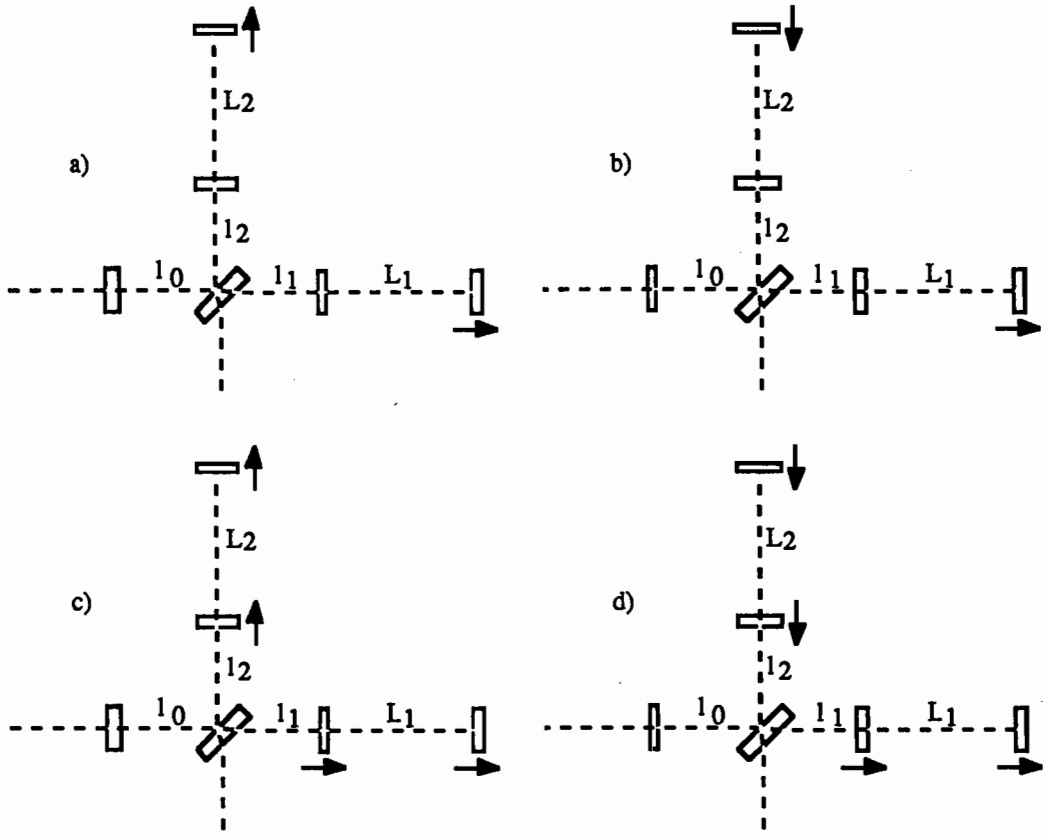

Fig. 3.1

For each of these independent displacements the signals at the output of several photodiodes, placed as shown in the picture below, (fig. 3.2) have been calculated. The modulation frequency used corresponds to one of the peaks in fig.2.3, i.e. the side bands are resonant in the recycling cavity and antiresonant in the Fabry-Perot.

The semi-transparent mirrors used to extract the beams monitored by the photodiodes 3, 4, 5, and 6 are assumed to reflect 10^{-4} of the incident light. This is necessary in order to keep as small as possible the losses inside the interferometer.

To extract the beam reflected by the recycling mirror a polarising beam-splitter joined with a quarter wave plate might be used; in this case one might be able to extract nearly all the reflected light. Since the use of these additional optical components may turn out to be

impossible, especially because of the change of polarisation inside the interferometer, in all the calculations that follow it is assumed to use a semi-transparent mirror extracting 1% of the reflected light.

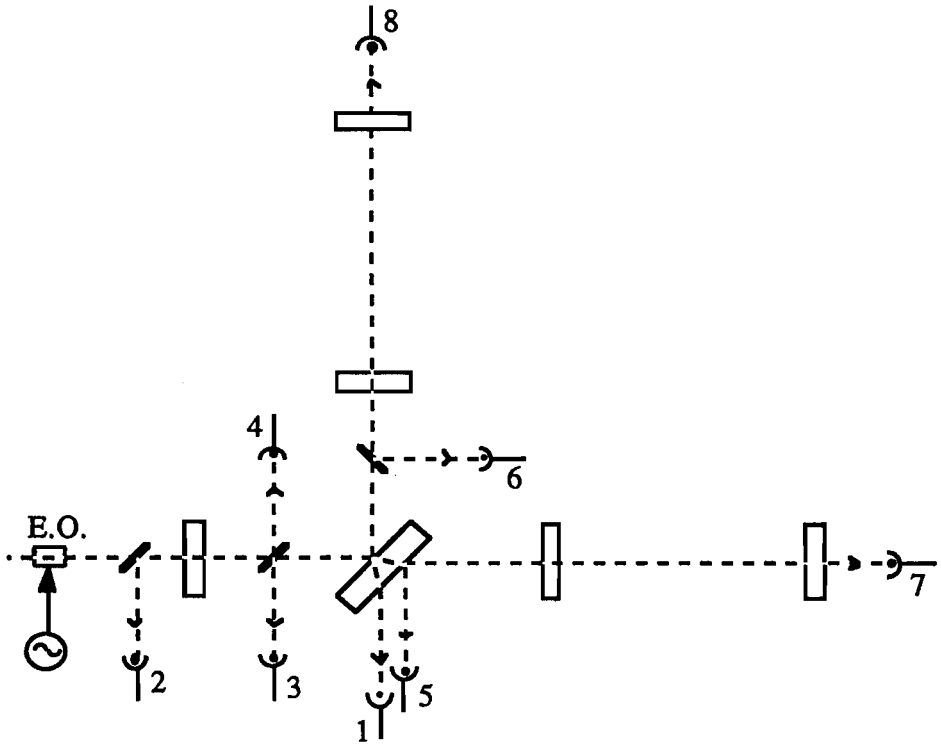

Fig. 3.2

The calculation has been carried out using the following parameters:

laser power	10 Watt
F-P finesse	≈ 40
recycling factor	≈ 100
ITF losses	1%
ITF contrast defect	10^{-4}
arms length	3 km
Michelson arm lengths	l_1=6.2m, l_2=5.8m, l_0=6m
Modulation frequency	≈ 6.27 MHz

The results are given in the following table, each row corresponding to a photodiode. The values given in the first four columns are the signals produced by mirror displacements equal to $\lambda/10^6$ (length changes of $2\lambda/10^6$). Apart from a normalisation factor, given in the fifth column, the two given numbers are the signal amplitude (in Watt) and its phase with respect to the modulation source.

For each photodiode the shot noise level (in $W/\sqrt{Hz}$) is given in the sixth column. It has been calculated assuming a stationary noise; any additional contribution, due to the non-stationary shot noise that affects an amplitude modulated beam [11], has been neglected.

	$\delta L_1 - \delta L_2$	$\delta L_1 + \delta L_2$	$\delta l_1 - \delta l_2$	$\delta l_1 + \delta l_2$	Normal.	Shot noise
1	1 0°	0 0°	4.1E-2 0°	0 0°	9.3E-3 135°	3.0E-10
2	2.3E-6 -90°	1 0°	5.6E-5 -90°	4.2E-2 0°	6.1E-4 180°	2.0E-11
3	1.4E-4 90°	1 0°	3.3E-3 90°	2.2E-2 180°	1.7E-3 180°	1.4E-10
5	1.0E-2 1°	1 0°	3.3E-3 90°	2.2E-2 180°	8.7E-4 -90°	1.0E-10
7	5.0E-3 2°	1 0°	3.3E-3 90°	2.2E-2 180°	8.8E-4 178°	4.6E-10

The output of photodiode 4 has not been reported in the table because it contains the same information as the one of photodiode 3. The signals from photodiode 6 and 8 (also not reported) may be deduced from the ones of photodiode 5 and 7 just by interchanging cavity 1 and 2.

As expected the signal at the output of the photodiode 1 is mainly related to the long Fabry-Perot's differential mode (δL_1-δL_2); its dependence on the Michelson differential mode (δl_1-δl_2) is 25 times smaller ($25=2F/\pi$, $F=40$).

On the contrary the photodiode 2 signal mainly depends on the long Fabry-Perot's common mode (δL_1+δL_2).

Also the in-phase signal of photodiode 3 mainly depends on the Fabry-Perot's common mode while the quadrature is dominated by the Michelson differential mode. The latter being much smaller than the first one, any error in the demodulating signal phase can make the in-quadrature component also more sensitive to the long Fabry-Perot's common mode.

The output of photodiode 4 contains the same information as the one of photodiode 3.

Photodiode 5 is the one which monitors the north arm cavity reflection but its output signal also depends strongly on the west arm cavity length. This effect is due to the coupling between the two Fabry-Perot's cavities, induced by the recycling mirror. Consequently it is mainly sensitive to the Fabry-Perot's common mode and its dependence on the Fabry-Perot's differential mode is 50 times smaller. The situation is similar for photodiode 6; the recycling makes the signals from these two photodiodes equal except for a 2% difference.

This coupling between the two Fabry-Perot cavities also affects the signals of the two photodiodes which monitor the Fabry-Perot transmission (7 and 8 in fig. 3.2). Consequently also these two signals are mainly related to the Fabry-Perot's common mode and not, as one might expect, only to the length variations of the cavity after which they are measured.

Furthermore, due to the low power that reaches these two photodiodes the signal to noise ratio is smaller compared to the case of the photodiodes which detect the Fabry-Perot's reflections.

In conclusion we see that most of the signals are more sensitive to the length variations of the Fabry-Perot's than of the short Michelson arms. To extract the information about the Michelson arms length difference and the recycling cavity length, we need to calculate the difference between two or more signals. This operation will decrease the signal to noise ratio, since detector's noises add incoherently when their signals are combined.

In order to proceed in the calculation four independent signals have been chosen and the effect on the signal-to-noise ratio of combining signals from various detector has been studied.

The signal of photodiode 1, photodiode 2 and the in phase and quadrature signals of photodiode 5 have been chosen because they all detect beams that are easily accessible in VIRGO. Even if linearly independent, the signals are strongly coupled and the coupling depends on the phase of the demodulating signal used for photodiode 5.

One possible feedback configuration is shown in figure 3.3. The signals from photodiodes 1 and 2, which have a higher signal-to-noise ratio, are used to control the cavity output mirrors, while the in phase and quadrature signals from photodiode 5 are used to control the recycling mirror and the beam-splitter.

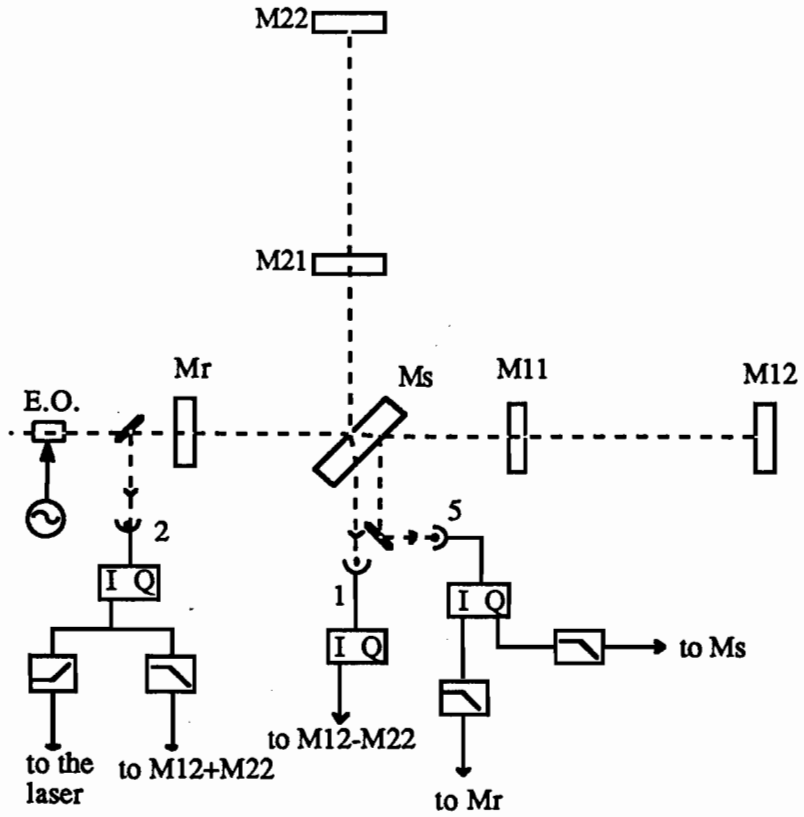

Fig. 3.3

One may think to a more general configuration where the various signals are combined before feeding them back to the mirrors, in order to obtain error signals depending only on the length to be controlled. In appendix B it is shown that in the high gain limit the final signal-to-noise ratio depends only on the relation between the signals and the displacements as expressed by the matrix given in the previous table and is independent on the way these signals are fed back to the mirrors. This means that it makes no difference (for the final noise level), whether "clean" error signals (depending only on one length at a time) are used to control the mirrors, or directly the "raw" signals as obtained from the diodes. If n_i is the noise affecting photodiode i, the minimum detectable variations for the lengths δx_i (with $\delta x_i = \delta L_1 - \delta L_2$, $\delta L_1 + \delta L_2$, $\delta l_1 - \delta l_2$, and $\delta l_1 + \delta l_2$) are given by the following relation:

$$\delta x_i^2 = (A^{-1})_{ij}^2 \, n_j^2 \quad . \tag{3.1}$$

A_{ij} being the matrix that gives the signal i produced by a variation of the length j.

By using the shot noise level of each detector the minimum detectable length variations (in $m/\sqrt{Hz}$) have been calculated. They are given in the table below.

$\delta L_1 - \delta L_2$	$\delta L_1 + \delta L_2$	$\delta l_1 - \delta l_2$	$\delta l_1 + \delta l_2$
3.0E-18	1.6E-19	7.5E-17	4.0E-18

The limit on δL_1-δL_2 corresponds to an h sensitivity of about $10^{-21}/\sqrt{Hz}$; this value is obviously spoiled due to reintroduction of noise by the feedback system. Consequently in order to reach the VIRGO sensitivity goals it cannot be allowed that all of the feedback loops work in the operating frequency range of the antenna.

From the shot noise level and the inverse matrix elements one observes that the main contribution to noise comes from photodiode 5 (Δl has been chosen equal to 0.4m to optimise the signal-to-noise ratio of this photodiode). In order not to introduce noise in the interferometer it is necessary to filter the output of this photodiode in the frequency range of interest of the antenna, thereby lowering the unity-gain frequency of the l_1/l_2 loops. On the other hand the output signals of photodiodes 1 and 2 have a better signal-to-noise ratio and so they can be used, even at higher frequency, to control the system. This is shown in figure 3.3.

The signal from photodiode 1 gives information on the Fabry-Perot's differential mode with a sensitivity (shot noise limited) equal to $\approx 6 \cdot 10^{-20}$ $m/\sqrt{Hz}$ that corresponds to $h \approx 2 \cdot 10^{-23}$. Consequently it can be used to control the cavity length difference with a large band (fig. 3.3) so that the feedback signal will directly contain the gravitational wave information.

The signal from photodiode 2 is directly related to the Fabry-Perot's common mode and the shot noise limits its sensitivity to $3 \cdot 10^{-20}$ $m/\sqrt{Hz}$. A laser frequency fluctuation $\delta\nu$ will produce a signal at photodiode 2 equal to the one produced by a Fabry-Perot's common mode displacement $\delta L_1 + \delta L_2 = (\delta\nu / \nu) \cdot (L_1 + L_2)$. Consequently the signal from photodiode 2 can be

used to stabilise the laser on the interferometer at high frequency. The shot noise affecting this detector will limit the frequency sensitivity of this system to $\delta\nu \approx 3 \cdot 10^{-9}$ Hz/$\sqrt{\text{Hz}}$, a value that fulfils the VIRGO specifications.

The overall stability of the control system remains to be studied and, in particular, the effect of the coupling between the various signals on its stability. Furthermore precise specifications on the gain and the on the bandwidth of the various loops still have to be defined. As already said, it is planned to lock the interferometer on the laser frequency at low frequency (let's say up to a few hundreds millihertz) and to do the opposite at higher frequency (from 10 Hz); it remains to understand what will happen in the intermediate frequency region (a few Hertz).

From the experimental point of view a locking scheme with simple frontal modulation is currently under study at Caltech [12]. The test is performed on a rigid recycled interferometer with a 6 meter long Fabry-Perot cavity in each arm. The apparatus is mounted on two optical tables and it is in air. The first results show that the system works, but a deeper analysis of the effect of the couplings on the overall signal-to-noise ratio still remains to be done.

IV Locking Scheme with Subcarrier

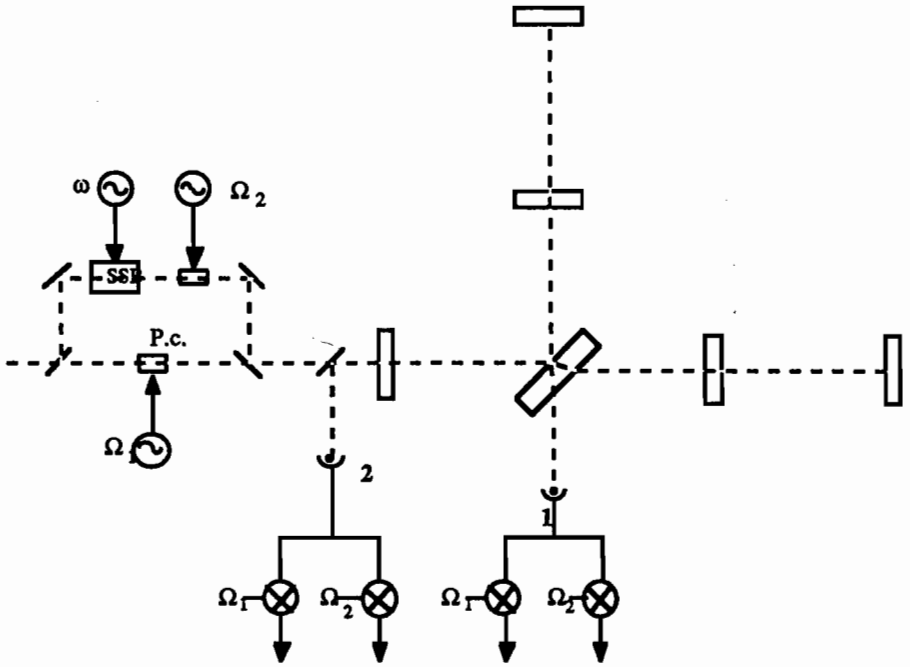

Fig.4.1: SSB modulation scheme

It is desirable to have a system in which the feedbacks for the various interferometer lengths act as much as possible as independent units. This simplifies understanding of the functioning of the system and facilitates troubleshooting, since all parameters can be accessed separately.

As we have seen in the last section, the signals in the case of the frontal modulation are not independent of each other. Especially, at all the diodes the signal is one to three orders of magnitude more sensitive to the FP lengthes L_1 and L_2 than to the short Michelson lengths $l_1$and l_2. The reason for this is, that the laser frequency itself is resonant in the Fabry Perot's. Therefore, the phase sensitivity of the reflected light to Fabry Perot's length changes is $2F/\pi$=25 times enhanced compared to the case of a Michelson length variation. The beat of the carrier and the (non-resonant) side bands (the demodulated signal) contains therefore the same strong dependency on L_1 and L_2.

Calculations show that this is still valid, if also the side bands are made resonant; contrary to what one might intuitively assume, no cancellation of the L_1/L_2 sensitivity occurs in the beat note between carrier and side bands.

If one wishes feedback circuits for the individual parameters that are more independent from each other, it is therefore necessary to have a system of carrier and side bands which all of them do not enter the arm cavities. This can be achieved with the scheme depicted in Fig.4.1. With a single side band (SSB) modulator a subcarrier is created, that, after being modulated with a suitable frequency, is added to the main laser beam, which itself is modulated as before.

The light impinging on the recycling mirror has the sideband structure shown in Fig.4.2a; the laser (main carrier) has two modulation side bands at $\pm\Omega_1$; the subcarrier is displaced with respect to the main carrier by ω and has two side bands at $\omega\pm\Omega_2$. The beating of the sidebands with their respective carriers now leads to diode currents modulated with Ω_1 and Ω_2, yielding signals which are predominantly sensitive to the long or short Michelson arms, respectively.

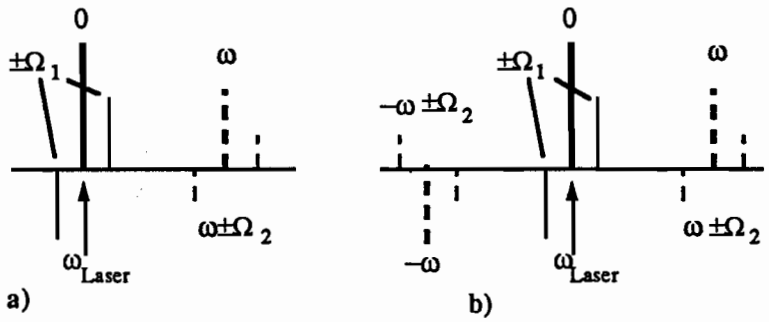

Fig.4.2: Frequency spectra for two subcarrier generation schemes.
a) single side band; b) phase modulation with suppressed carrier

The frequency Ω_1 is defined by the discussion of the last chapter. The subcarrier must have a dark fringe at the output, which corresponds to the condition

$$\omega = n\frac{\pi c}{\Delta l} \quad (n \in \mathbf{N}) \quad , \tag{4.1}$$

giving $\omega/2\pi$ = 187.5 MHz as the lowest possible frequency (n=1) for Δl =0.8m. If one allows for a small detuning of the arm cavities, then one may deviate up to ±5-10% from the exact condition (see appendix C).

The subcarrier must not have a resonant power build-up in the arm cavities. In order to achieve good recycling, the phase shift upon reflection off the FP must be well defined (ideally 0°), which leads to the stronger requirement, that the FP must be antiresonant:

$$L_{1/2} = (m+0.5)\frac{\pi c}{\omega} = (m+0.5)\cdot\frac{\Delta l}{n} \quad (m \in \mathbf{N}) \tag{4.2}$$

In our case, this can be achieved with a FP length of 3000.4 m, while maintaining the main carrier resonance. Again, this condition needs not being fulfilled exactly, if the FP's are allowed to be a bit detuned.

For the modulation, the next frequencies being recycled while antiresonant in the FP's ($\Phi(\omega_l+\omega\pm\Omega_2)\approx 0$) are multiples of the recycling cavity FSR away from the subcarrier frequency

$$\Omega_2 \approx n\cdot\frac{\pi c}{l_r} \quad , \tag{4.3}$$

leading to a lowest possible $\Omega_2 \approx 2\pi\cdot 12.5$ MHz for the parameters used. Other resonances in the neighborhood may also be used as long as the power inside the arm cavities remains small.

If we assume a tolerable loss of 5% for the main laser beam in order to provide the power for the SSB branch, then we get for the two "deviation" beam splitters a reflectivity of 2.5%, yielding a power in the SSB region after recombination of 6.25 mW.

We assume for simplicity that the SSB modulator transfers 100% of the incident carrier to the new subcarrier frequency.

The optimum modulation index m_{opt} is determined by demanding that the signal-to-noise ratio for l_1-l_2 at the interferometer exit is optimised. The signal itself increases with the product of subcarrier and sub-sideband amplitudes, i.e. to first order (for weak modulation) proportional to m. In the case of simple frontal modulation, the shot noise is determined by the power of the side bands inpinging on the detector, and is proportional to m also; here, however, it is dominated by the main carrier sidebands, and thus essentially constant. Consequently, m can be higher than in the case of the simple frontal modulation. A numerical calculation shows m_{opt} to be around 1.1.

In order to obtain the four required length informations, only two diodes are required, whose outputs must de demodulated with each of both modulation frequencies. The tables below show the parameters used and the calculated signals for this case. As can be seen, there is now essentially one diode/frequency combination for each of the parameters to be controlled; the coupling factor of $L_{1/2}$ in the $l_{1/2}$ signals and vice versa is now only $\pi/2F = 1/25$, so that for the feedback dynamics they can to first order be considered independent.

Laser power	10 Watt
Deviation beam sp. reflectivity	2.5 %
SSB generation efficiency	100%
D2 beam sp. reflectivity	1 %
Arm length	3000.4 m
Main modulation frequency	≈ 6.27 MHz
Subcarrier frequency	187.5 MHz
Subc. modulation frequency	≈12.49 MHz
δl per mirror	$10^{-6}\,\lambda$

Parameters used for the calculation

The minimum detectable length changes are determined by the signal strength and the shot noise of the DC current on the diode. For diode 1, the DC current is caused by the residual carrier present due to imperfect contrast, and by the side band power coupled out with the Δl asymmetry. At diode 2, the DC current is caused by carrier and side bands reflected due to imperfect impedance matching of the recycling mirror; since the recycling mirror reflectivity

can be chosen appropriately, this contribution is quite small. The calculated results are included in the table.

Diode	$\delta L_1 - \delta L_2$	$\delta L_1 + \delta L_2$	$\delta l_1 - \delta l_2$	$\delta l_1 + \delta l_2$	Normal.	Shot noise
1 (Ω_1)	**1** 0°	0	4.1E-2 0°	0	1.1E-2 -135°	3.6E-10
2 (Ω_1)	0	**1** 0°	2.9E-4 90°	3.8E-2 0°	6.8E-5 180°	3.6E-12
1 (Ω_2)	4.1E-2 0°	0	**1** 0°	0	8.0E-7 180°	3.6E-10
2 (Ω_2)	4.2E-4 -90°	4.1E-2 0°	1.1E-2 -90°	**1** 0°	1.3E-7 180°	3.6E-12

Signal matrix for SSB modulation [W and W/$\sqrt{\text{Hz}}$]

Diode	$\delta L_1 - \delta L_2$	$\delta L_1 + \delta L_2$	$\delta l_1 - \delta l_2$	$\delta l_1 + \delta l_2$
1 (Ω_1)	**6.8E-20**	∞	1.7E-18	∞
2 (Ω_1)	∞	**1.1E-19**	3.6E-16	2.8E-18
1 (Ω_2)	2.3E-14	∞	**9.1E-16**	∞
2 (Ω_2)	1.3E-13	1.3E-15	5.2E-15	**5.4E-17**

Sensitivity matrix for SSB modulation [m/$\sqrt{\text{Hz}}$] (low gain limit)

As before, the formula derived in appendix B can be used to calculate the shot noise limited displacement sensitivities assuming high gain feedback for all diodes/lengths. The result is shown in the following table.

$\delta L_1 - \delta L_2$	$\delta L_1 + \delta L_2$	$\delta l_1 - \delta l_2$	$\delta l_1 + \delta l_2$
2.6E-17	1.5E-18	6.5E-16	3.9E-17

Sensitivity matrix for SSB modulation [m/$\sqrt{\text{Hz}}$] (high gain limit)

From this we can see that the feedbacks involving the noisy signals at Ω_2 must be slow in order to avoid that the important signals are spoiled. A possible configuration is shown in fig. 4.3.

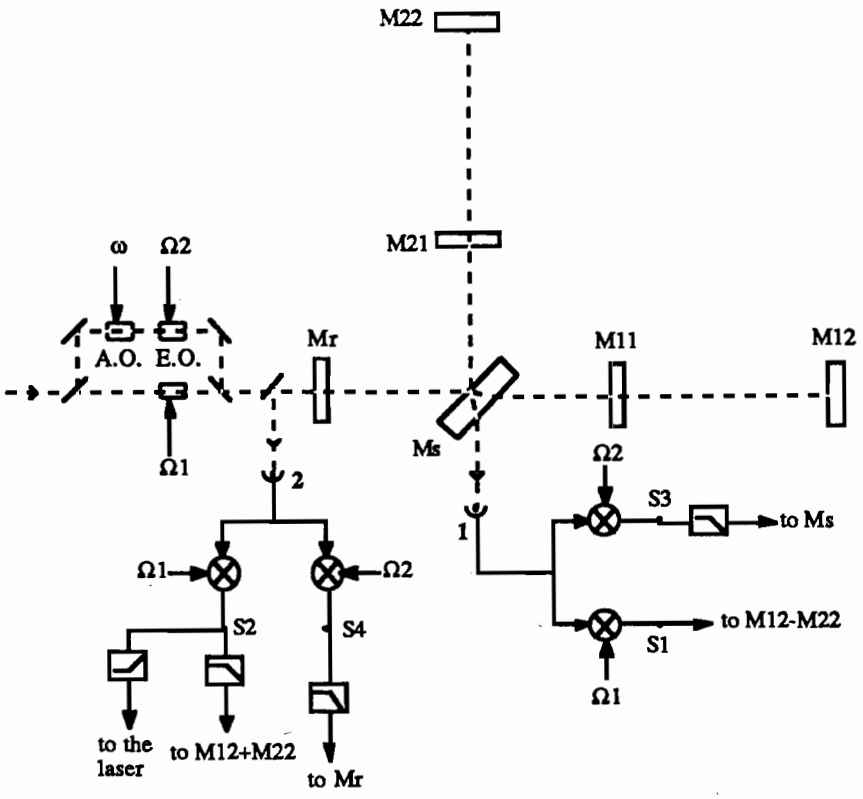

Fig. 4.3: Feedback configuration for SSB modulation scheme

The subcarrier modulation scheme seems quite promising for an application in VIRGO. One disadvantage with repect to the simple frontal modulation is however, that the sideband generation scheme introduces an additional complication: according to scheme 4.1, two phase modulators and one SSB generator (typically an acousto-optic modulator, AOM) are needed.

A simpler possibility is depicted in Fig. 4.4; here the AOM is replaced by a phase modulator, fed with a voltage oscillating at ω. Thus, two subcarriers at $\pm\omega$ are generated. The second Pockels cell then modulates both of them with Ω_2. The modulation index m for ω is chosen such, that the carrier in the upper path is suppressed ($J_0(m) = 0$ for m=2.4). This is important, because otherwise the carrier itself will be modulated at Ω_2, and thus in the final signal at this frequency there will again be a contribution coming from light that has penetrated into the FP's. The resulting total frequency spectrum at the interferometer input is shown in Fig. 4.2b. The signals due to the two subcarriers add up with the right sign and thus give a signal twice as high. The two modulators for ω and Ω_2 can be replaced by one that receives the sum of the two driving voltages.

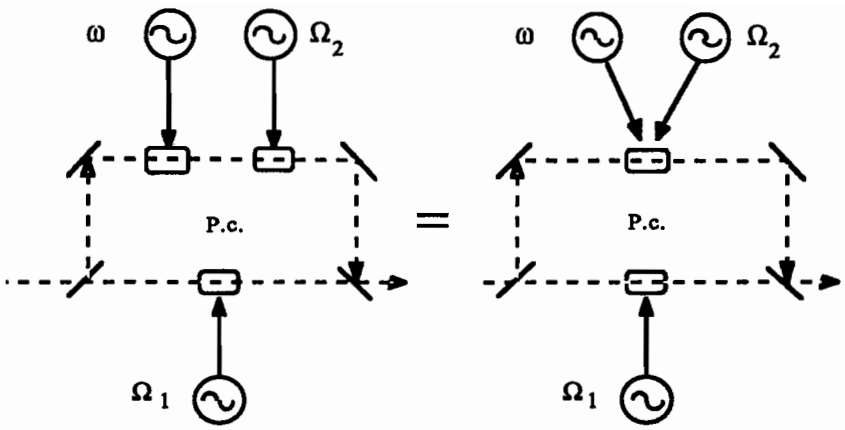

Fig. 4.4: Alternative subcarrier generation scheme

A scheme allowing the generation of a sideband structure similar to the one shown in Fig. 4.2b without the use of a bypass structure is presently being investigated. Such a scheme would allow a higher power in the subcarrier branch and thereby a better noise limited sensitivity.

References

[1] A.Brillet; VIRGO note on servo systems, 23/01/93

[2] A.Brillet, A.Giazotto; VIRGO proposal, (1989)

[3] R.Weiss; Q.Prog. Rep. Lab. Electron. MIT **105**, 54, (1972)

[4] A.Billing, K.Maischberger, A.Rüdiger, R.Schilling, L.Schnupp, W.Winkler; J.Phys.E **12**, 1043, (1979)

[5] R.W.P.Drever; in Gravitational Radiation, Les Houches 1982, eds. N.Deruelle and T.Piran (North-Holland Amsterdam, 1983) pp. 321-338

[6] C.N.Man, D.Shoemaker, MPham Tu, D.Dewey; Phys.Lett.A **148**, 8, (1990)

[7] A.Brillet, A.Giazotto; VIRGO final conceptual design, (1992)

[8] A.Brillet; VIRGO plenary meeting, Orsay, December 1992

[9] L.Schnupp; Workshop on G.W. detectors, Munich, Mai 1988

[10] C.N.Man; VIRGO note PJT92 033a, (1992)

[11] T.M.Niebauer, R.Schilling, K.Danzmann, A.Rüdiger, and W.Winkler; Phys.Rev.A, (1990)

[12] F.Raab; VIRGO-LIGO meeting, Lyon-Orsay, July 1993

Appendix A

This appendix contains the calculation which leads to the results shown in section II. The complete algebra of a recycled Fabry-Perot interferometer in frontal modulation configuration is developed.

Consider the case of an interferometer illuminated with a monochromatic laser beam of amplitude A_0 and frequency ω_0. Through an electro-optic modulator the laser beam is phase modulated with a frequency Ω so that an infinite number of sidebands are generated. If the modulation amplitude m is little enough one can consider only first order sidebands and the field A_i incident on the recycling mirror is well described by the following well known expression:

$$A_i(t) = A_0 \left[J_0(m)\, e^{i\omega_0 t} + J_1(m)\, e^{i(\omega_0+\Omega)t} - J_1(m)\, e^{i(\omega_0-\Omega)t} \right] \qquad (A.1)$$

The field amplitudes inside the recycling cavity as well as the one transmitted at the output port of the interferometer depend on the frequency one is considering.

As shown in fig.A.1, the field inside the recycling cavity ($A_{rec}(\omega)$) is given by the superposition of the light that is transmitted through the recycling mirror and the light that comes back from the two interferometer arms and is reflected on the recycling mirror.

$$A_{rec}(\omega) = t_r\, A_i(\omega) - r_r\, A_{back}(\omega) \qquad (A.2)$$

where r_r and t_r are the reflectivity and transmittivity of the recycling mirror.

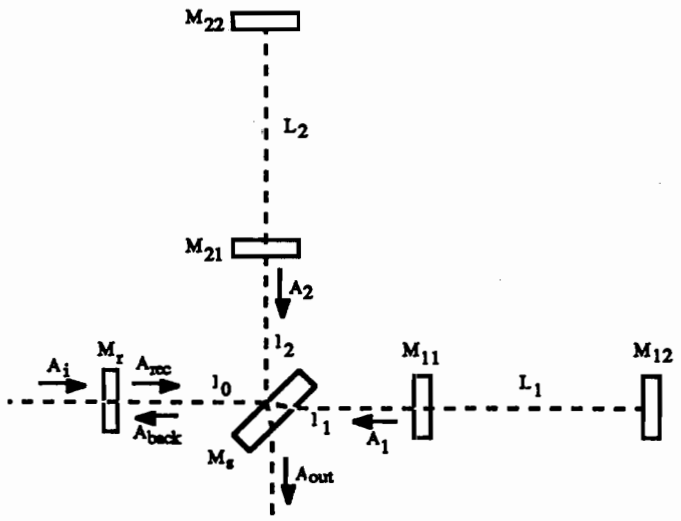

Fig. A.1

The field $A_{back}(\omega)$ reflected back from the beam-splitter is equal to the field $A_{rec}(\omega)$ at the recycling mirror after one trip inside the whole interferometer:

$$A_{back}(\omega) = e^{-i\,\omega\frac{2\,l_0}{c}}\left[r_s^2\, e^{-i\,\omega\frac{2\,l_2}{c}}\, r_2(\omega)\, e^{i\,\phi_2} + t_s^2\, e^{-i\,\omega\frac{2\,l_1}{c}}\, r_1(\omega)\, e^{i\,\phi_1}\right] A_{rec}(\omega) \quad (A.3)$$

being r_s and t_s the transmittivity and reflectivity of the beam splitter. The quantity $r_1(\omega)\, e^{i\phi_1(\omega)}$ ($r_2(\omega)\, e^{i\phi_2(\omega)}$) represents the complex amplitude reflectivity of cavity 1 (cavity 2), and depends on the frequency one is considering. Using equations (A.2) and (A.3) the following solution is found for the field A_1 inside the recycling cavity:

$$A_{rec}(\omega) = \frac{t_r\, A_i(\omega)}{1 + r_r\, e^{-i\,\omega\frac{2\,l_0}{c}}\left[r_s^2\, e^{-i\,\omega\frac{2\,l_2}{c}}\, r_2(\omega)\, e^{i\,\phi_2(\omega)} + t_s^2\, e^{-i\,\omega\frac{2\,l_1}{c}}\, r_1(\omega)\, e^{i\,\phi_1(\omega)}\right]} \quad (A.4)$$

For the carrier ω_0, which is resonant inside the recycling cavity as well as in the Fabry-Perot's, the following conditions are fulfilled:

$$\frac{\omega_0}{c}(2\,l_0 + 2\,l_1) = 0; \quad \frac{\omega_0}{c}(2\,l_0 + 2\,l_2) = 0 \pmod{2\pi} \quad (A.5)$$

$$\phi_1(\omega) = \pi; \quad \phi_2(\omega) = \pi \pmod{2\pi}$$

If, for sake of simplicity, the beam-splitter is assumed to be symmetrical (r_s=t_s) as well as the two Fabry-Perot's ($r_1(\omega_0)$=$r_2(\omega_0)$ and $\phi_1(\omega_0)$=$\phi_2(\omega_0)$), the carrier field amplitude inside the recycling cavity is given by the well known formula:

$$A_{rec}(\omega_0) = \frac{t_r}{1 - r_r\, r(\omega_0)}\, A_i(\omega_0) \quad (A.6)$$

showing that the carrier amplitude inside the recycling cavity is equal to the input amplitude multiplied by the square root of the recycling factor.

Using again conditions (A.5) and equation (A.4) we find that the sideband amplitudes are given by the following expression:

$$A_{rec}(\omega_0 \pm \Omega) = \frac{t_r\, A_i(\omega_0 \pm \Omega)}{1 + r_r\, r(\omega_0 \pm \Omega)\, e^{\pm i\frac{\Omega}{c}2\,l_r}\, e^{i\,\phi\,(\omega_0 \pm \Omega)}\cos\left(\frac{\Omega}{c}\Delta l\right)} \quad (A.7)$$

with:
$$l_r = l_0 + \frac{l_1 + l_2}{2} \quad \text{and} \quad \Delta l = l_1 - l_2 \quad (A.8)$$

In order to maximize the sideband amplitudes, and consequently the effective modulation depth inside the recycling cavity, the following condition must hold:

$$-\frac{\Omega}{c}2\,l_r + \phi(\omega+\Omega) = \pi \pmod{2\pi} \quad (A.9)$$

This means that to transmit the sidebands through the interferometer the frequency of modulation must be carefully chosen to be efficiently recycled inside the recycling cavity. When condition (A.9) is fulfilled the sideband amplitudes pass through the maxima shown in fig. 2.2 and 2.3.

Using equations (A.6) (A.7) and (A.9) the total field amplitude inside the recycling cavity can be calculated:

$$\begin{aligned} A_{rec}(t) &= \frac{t_r\, J_0(m)\, A_0}{1 - r_r\, r(\omega_0)}\; e^{i\omega_0 t} \\ &+ \frac{t_r\, J_1(m)\, A_0}{1 - r_r\, r(\omega_0+\Omega)\cos\left(\frac{\Omega}{c}\Delta l\right)}\; e^{i(\omega_0+\Omega)t} - \frac{t_r\, J_1(m)\, A_0}{1 - r_r\, r(\omega_0-\Omega)\cos\left(\frac{\Omega}{c}\Delta l\right)}\; e^{i(\omega_0-\Omega)t} \\ &= \frac{t_r\, A_0}{1 - r_r\, r(\omega_0)}\; e^{i\omega_0 t} \\ &\cdot \left[J_0(m) + \frac{(1 - r_r\, r(\omega_0))\, J_1(m)}{1 - r_r\, r(\omega_0+\Omega)\cos\left(\frac{\Omega}{c}\Delta l\right)}\; e^{i\Omega t} - \frac{(1 - r_r\, r(\omega_0))\, J_1(m)}{1 - r_r\, r(\omega_0-\Omega)\cos\left(\frac{\Omega}{c}\Delta l\right)}\; e^{-i\Omega t} \right] \end{aligned} \qquad (A.10)$$

For small modulation $J_0(m)\approx 1$ and $J_1(m)\approx m/2$, and the equation (A.10) simplifies to:

$$A_{rec}(t) = \frac{t_r\, A_0}{1 - r_r\, r(\omega_0)}\; e^{i\left[\omega_0 t + \frac{(1 - r_r\, r(\omega_0))}{1 - r_r\, r(\omega_0+\Omega)\cos\left(\frac{\Omega}{c}\Delta l\right)}\, m \sin(\Omega t)\right]} \qquad (A.11)$$

from which one sees that even if the optimum condition (A.9) is satisfied, the effective modulation amplitude inside the recycling cavity is reduced by the factor $(1 - r_r\, r(\omega_0)) / (1 - r_r\, r(\omega_0+\Omega)\cos(\frac{\Omega}{c}\Delta l))$.

Let's now calculate the field transmitted at the output port of the interferometer. The output field is the superposition of the two beams reflected from the two arms of the interferometer A_1 and A_2 that are related to the field inside the recycling cavity by the following expression:

$$A_{1,2}(\omega) = A_{rec}(\omega)\, e^{i\frac{\omega}{c} l_0}\, t_s\, r_s\, e^{i\frac{\omega}{c} 2 l_{1,2}}\, r_{1,2}(\omega)\, e^{i\,\phi_{1,2}(\omega)} \qquad (A.12)$$

Using the equation (A.10), (A.12) and assuming a weak modulation one finds the following expression for the amplitude of the fields A_1 and A_2 reflected by the two arms of the interferometer:

$$\begin{aligned} A_{1,2}(t) &= \frac{t_r\, r_s\, t_s\, r(\omega_0)\, A_0}{1 - r_r\, r(\omega_0)} \\ &\cdot e^{i\left[\omega_0\left(t - \frac{l_0+2l_{1,2}}{c}\right) + \phi_{1,2} + \frac{(1 - r_r\, r(\omega_0))}{1 - r_r\, r(\omega_0+\Omega)\cos\left(\frac{\Omega}{c}\Delta l\right)}\, m \sin\left[\Omega\left(t - \frac{l_0+2l_{1,2}}{c}\right)\right]\right]} \end{aligned} \qquad (A.13)$$

By adding these two fields one obtains the field transmitted at the output port of the interferometer; the modulus square of the quantity so obtained represents the power impinging on the photodiode:

$$P_{out} = \frac{1}{2}\left(\frac{t_r\, r(\omega_0)}{1 - r_r\, r(\omega_0)}\right)^2 |A_0|^2 \cdot \left[1 + C\cos\left(\Delta\phi + \frac{\omega_0}{c}\Delta l + \frac{2\sin\left(\frac{\Omega}{c}\Delta l\right)(1 - r_r\, r(\omega_0))}{1 - r_r\, r(\omega_0+\Omega)\cos\left(\frac{\Omega}{c}\Delta l\right)} m\cos(\Omega t)\right)\right] \quad \text{(A.14)}$$

where C is the interferometer output contrast and $\Delta\phi=\phi_2-\phi_1$.
From the equation (A.14) one sees that the output phase of the interferometer is modulated with an amplitude equal to:

$$\frac{2\sin\left(\frac{\Omega}{c}\Delta l\right)(1 - r_r\, r(\omega_0))}{1 - r_r\, r(\omega_0+\Omega)\cos\left(\frac{\Omega}{c}\Delta l\right)} m \quad \text{(A.15)}$$

For a given input modulation amplitude m the output modulation amplitude is maximum when Δl satisfy the following condition:

$$\cos\left(\frac{\Omega}{c}\Delta l\right) = r_r\, r(\omega_0+\Omega) \quad \text{(A.16)}$$

The equation (A.16) means that for a given modulation frequency Ω it exists an optimum Δl which maximises the transmission of the sidebands at the output port of the interferometer as is shown in fig.2.4 and 2.5. In effect if one reduces too much Δl the sidebands are more efficiently recycled (as equation A.10 shows) but only a little part of this amplitude is transmitted at the output port. On the other hand if one increases Δl the transmission of the sidebands to the output port of the interferometer increases but the they are less efficiently recycled so that the effective sidebands amplitude reaching the photodiode decrease. Equation A.16 represents the compromise between these two effects.

Appendix B

Assume that n variables x_j (j=1,n) are to be controlled and that these variables are monitored with n detectors each one giving a signal s_i related to the n variables through the matrix A_{ij}.

Moreover assume that each detector is affected by a noise level n_i and that all these noises are uncorrelated; the following relation holds:

$$s_i = A_{ij}\, x_j + n_i \quad ;$$

here we are summing over equal indices. These n signals s_i are then combined (fig. B.1) with a matrix operator B_{ij} and each output thus obtained is then amplified and filtered with a frequency response $g_i(\omega)$. The n signals so obtained are fed back to the n variables x_i. The system is thus described by the following system of equations:

$$x_i = x_i^{(o)} - g_i(\omega)\, B_{ij}\, (A_{jk}\, x_k + n_j) \quad , \qquad \text{(B.1)}$$

where $x_i^{(o)}$ represents the free evolution of the variable x_i when the feedback is off.

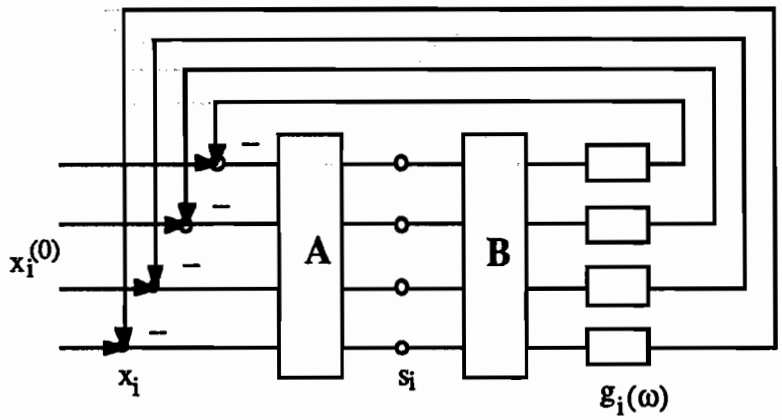

Fig. B.1

Equation B.1 may be written in the following form:

$$(\delta_{ik} + g_i(\omega)\, B_{ij}\, A_{jk})\, x_k = x_i^{(o)} - g_i(\omega)\, B_{ij}\, n_j \qquad \text{(B.2)}$$

Consider now the high gain limit $g_i(\omega)\, B_{ij}\, A_{jk} \gg \delta_{ik}$. Using this condition the solution of equation B.2 becomes:

$$x_i = (A^{-1}\, B^{-1}\, g(\omega)^{-1})_{ij}\, x_j^{(0)} - (A^{-1})_{ij}\, n_j \qquad \text{(B.3)}$$

which shows that the noise is reintroduced through the term A^{-1} independently of the way the signals are recombined (matrix B). If the noises on the various detectors are not correlated, the variable x_i can be controlled with an accuracy given by the following relation:

$$\delta x_i^2 = (A^{-1})_{ij}^2\, n_j^2 \quad ; \qquad \text{(B.4)}$$

that is the formula used in the text.

Appendix C

The conditions for the subcarrier scheme can be determined by the following consideration. The carrier (laser frequency, ω_l) and the subcarrier must both have a dark fringe at the output and be resonant in the recycling cavity. The first condition writes

$$\frac{2\Delta l}{c}x + \Phi_1(x) - \Phi_2(x) = \pi + m_x \cdot 2\pi \quad \text{(dark fringe)} \qquad \text{(C.1)}$$

where $x=\omega_l$ or $\omega_l+\omega$, and $\Phi_k(x)$ is the phase shift encountered by a beam reflected off arm cavity k[1].

The carrier and subcarrier should have a high and low power build-up in the FP's, respectively. Let us assume, that they are near resonance / antiresonance, with a detuning of a fraction of a wavelength $\pm\delta L$. Then we have

$$\Phi_{1/2}(\omega_l) \approx \pi \pm 4\pi\frac{\delta L}{\lambda}\cdot\frac{2F}{\pi} = \pi \pm \frac{8\delta LF}{\lambda} \qquad \text{(res.)}$$

$$\Phi_{1/2}(\omega_l+\omega) \approx \pm 4\pi\frac{\delta L}{\lambda}\cdot\frac{\pi}{2F} = \pm\frac{2\pi^2\delta L}{\lambda F}\ , \qquad \text{(antires.)}$$

and (C.1) yields by subtraction the dark fringe condition for ω:

$$\frac{2\Delta l}{c}\cdot\omega + \frac{4\delta L}{\lambda}\cdot\left(\frac{\pi^2}{F} - 4F\right) = n\cdot 2\pi \quad (n := m_1 - m_2 \in \mathbb{N}). \qquad \text{(C.2)}$$

For $\delta L=0$, this reduces to the ideal condition $\omega = n\cdot(\pi c/\Delta l)$ (perfect antiresonance), giving $\omega/2\pi$ = 187.5 MHz as the lowest possible frequency (n=1) for Δl=0.8 m. The maximum allowable δL is given by the resonance requirement for the main carrier: $\delta L < \varepsilon\cdot$ HWHM = $\varepsilon\lambda/4F$, with e.g. ε=10%. The antiresonance condition for the subcarrier is much weaker, since we demand only that there is no power build-up in the FP's.

The recycling condition is

$$\pi\frac{1+\text{sign}\cos(x\Delta l/c)}{2} + \frac{2l}{c}x + \frac{\Phi_1(x)+\Phi_2(x)}{2} = j_x\cdot 2\pi\ . \quad \text{(recycling)} \qquad \text{(C.3)}$$

The first term keeps track of the phase reversals occuring when Δl is swept. If again we assume resonance/antiresonance with a small (in-phase) detuning δL, we have

$$\Phi_k(\omega_l) \approx \pi + \frac{8\delta LF}{\lambda} \quad \text{and} \quad \Phi_k(\omega_l+\omega) \approx \frac{2\pi^2\delta L}{\lambda F}\ .$$

Then the condition for ω is

$$\frac{2l\omega}{c} + \frac{2\delta L}{\lambda}\cdot\left(\frac{\pi^2}{F} - 4F\right) + \pi\cdot\frac{1+\text{sign}\cos(\omega\Delta l/c)}{2} = n\cdot 2\pi\ , \qquad \text{(C.4)}$$

from which we can again see that small errors in the recycling condition can be compensated by small detunings of the FP lengths and vice versa.

---

[1] $\Phi_k(x) = \arg\left(R_1 - r_1r_2\,(1+R_1)\cos\rho + R_1R_2 + i\cdot r_1r_2\,(R_1-1)\sin\rho\right)$, $\rho = x\backslash F(2L_k,c)$